International Journal of Innovative
Computing, Information and Control
Volume **13**, Number **2**, April **2017**

ICIC International ©2017 ISSN 1349-4198
pp. 509–520

AN IMPROVED CURVELET THRESHOLDING DENOISING ALGORITHM FOR ASTRONOMICAL IMAGE

Jie Zhang and Xiaoping Shi

Control and Simulation Center
Harbin Institute of Technology
No. 2, Yikuang Street, Nangang District, Harbin 150080, P. R. China
quhn1234@163.com; sxp@hit.edu.cn

Received October 2016; revised February 2017

Abstract. *In astronomical image processing, to solve the problem of slow convergence speed and poor denoising performance in compressed sensing iterative curvelet thresholding (ICT) algorithm, an improved ICT reconstruction algorithm with high performance is proposed. A Dai-Yuan stepsize is used by algorithm to accelerate its convergence speed. To improve the quality of the reconstructed image, a new curvelet threshold is proposed to select the curvelet coefficients of astronomical image. Meanwhile, the total variation method is employed to adjust the reconstructed image in each iteration for suppressing the pseudo-gibbs effect in the reconstructed image. Number experimental results demonstrate that the algorithm proposed is superior to the traditional ICT algorithm, which can achieve better denoising performance with a fast convergence speed and effectively protect the image detailed features. Furthermore, even with a lower compression ratio, the proposed algorithm can still obtain a higher peak signal to noise ratio (PSNR).*
Keywords: High resolution, Compressed sensing, Curvelet thresholding, Denoising, Astronomical image

1. **Introduction.** Research on astronomical image plays an important role in astronomy, which is a direct way to get astronomical information. However, since the high resolution astronomical image acquired by CMOS or CCD camera is often contaminated by noise when they are transmitted from the satellite to the earth station, it is inconvenient to distinguish the detailed feature in the astronomical image from the received image. Therefore, the image denoising method is often used to remove noise while retaining the important image features as much as possible. However, for high dimensional signal, due to the lack of enough valid data or the prior information of the signal, most denoising methods might fail to restore a high quality signal [1, 2]. To solve the problem of high dimensional signal reconstruction effectively, the scientists have been exploring an intrinsic low dimensional structure in high dimensional signal, and then the original high dimensional signal can be accurately reconstructed only by using the low dimensional structure. Sparsity [3, 4] is probably the easiest model for making full use of reduced dimensionality.

Based on the sparsity of the signal, Donoho proposed a new sampling theory: compressed sensing (CS) [1, 2, 3, 5] in 2006. It states that if a signal is sparse or compressible, then it can be accurately reconstructed only by using a few observations. To be specific, if the signal is sparse in a sparsity transform, a low measurement matrix can be used to sample the signal. At the same time, the original signal can be accurately recovered from these few observations by using a reconstruction algorithm. The tradition Shannon/Nyquist sampling theorem requires the sampling rate at least two times faster than the signal bandwidth, whereas the CS does not need to obey it. The CS theory mainly

consists of three important parts: sparsity transform, measurement matrix and the reconstruction algorithm. In this paper, what is focused is how to design a reconstruction algorithm with high performance.

After several years of development, many recovery algorithms have been presented, such as iterative shrinkage/thresholding (IST) algorithms [6, 7, 8, 9], linear programming methods [10, 11], gradient decreasing methods [12], nonconvex algorithm [13], and greedy pursuits methods [14]. Among these CS reconstruction algorithms, IST algorithms are often used by the scholars for signal reconstruction since it is very universal and quite simple to be implemented. Additionally, most sparse transforms can be easily incorporated to the IST framework. These advantages make it one of the most effective tools for dealing with the linear inverse problem. However, the IST methods do not function very well in terms of the denoising performance. Through the analysis of IST algorithms, it can be found that most of them mainly use the wavelets for sparse representation. However, the curvelet [15] has better sparse performance than that of wavelet. In the curvelet domain, the signal corresponds to the relatively large curvelet coefficient while noise corresponds to the small curvelet coefficient. Therefore, the curvelet thresholding method [15, 16] can remove the noise in the original image more effectively.

Based on the advantage of curvelet transform, various CS iterative curvelet shrinkage/thresholding (ICT) reconstruction algorithms have been proposed for solving the problem of signal denoising and reconstruction. For example, ICT algorithm with chi-squared cumulation distribution function [17] and ICT sparse reconstruction algorithm [18] can achieve better image denoising performance; the two-step ICT algorithm [19] and improved ICT algorithm [20] are proposed for remote sensing image denoising which can bring good results; iterative curvelet algorithm based on the adapt bivariate shrinkage threshold [21], compressed sensing seismic data denoising ICT method [22] and iterative 3D curvelet thresholding method [23] is put forward for seismic data denoising, which can effectively remove the noise in seismic data. From the research on these algorithms, the following problems are considered.

(1) Most scholars mainly focus on the denoising and reconstruction performance, but the convergence speed of the algorithm is very slow. For an excellent denoising reconstruction algorithm, fast convergence speed is very important.

(2) The image reconstructed by the thresholding denoising methods will result in the false gibbs phenomenon due to the lack of translation invariance property of curvelet transform, it is difficult to obtain some important image details from the reconstructed image. However, the image detail features are very important in the analysis of astronomical images. Therefore, it is very necessary to suppress the false gibbs phenomenon in astronomical image denoising.

This paper proposes a high performance improved ICT algorithm for suppressing the false gibbs phenomenon and improving the convergence speed of ICT algorithm. At the same time, the algorithm proposed is applied for solving the problem of astronomical image denoising and reconstruction. In this paper, the Dai-Yuan stepsize [24, 25] is used to solve the problem of the convergence speed of the algorithm proposed, which can effectively accelerate the convergence speed of the steepest descent method. To further improve the denoising performance in the algorithm proposed, a new curvelet threshold with high performance is proposed to select the curvelet coefficient of the original image. In remote sensing image denoising and reconstruction, the total variation (TV) method [26] can effectively suppress the false gibbs phenomenon. Therefore, this paper uses the TV method to adjust the reconstructed image in each iteration. By combining the above techniques, the algorithm proposed can achieve better denoising performance

and faster convergence speed. To confirm the validity of the proposed algorithm, the detailed theoretical analysis, simulation and experiments are performed.

The remainder of this article is organized as follows. In Section 2, the basic theoretical knowledge is introduced. The algorithm research and design are presented in Section 3. Afterwards, to demonstrate the effectiveness of the proposed algorithm, number experiments on high resolution astronomical images are shown in Section 4. Finally, the conclusions are drawn in Section 5.

2. The Basic Theoretical Knowledge.

2.1. The CS denoising model.

The classical denoising problem can be stated as follows:

$$y = x + e, \tag{1}$$

where x represents the original signal of size $N \times 1$, e denotes the noise which is generally considered as Gauss white noise and y is the $N \times 1$ noisy observations. For high dimensional signal, it is difficult to obtain enough valid information of the original signal from the high dimensional noisy observations since the value of N is very large.

In this article, high dimensional signal denoising with incomplete measurements is considered, which reads

$$y = \Phi x + e. \tag{2}$$

Here, Φ is an $M \times N$ ($M << N$) CS measurement matrix. It can be found that the recovery of the original signal x is an ill-conditioned linear inverse problem since $M << N$. However, the CS states that the original signal x can be reconstructed with high accuracy from the few observations y if x can be represented by a sparsity transform Ψ and if the measurement matrix Φ satisfies the restricted isometry property (RIP) [4, 10, 27]. In such a condition, Formula (2) can be rewritten as

$$y = \Phi x + e = \Phi\Psi\Psi^{-1}x + e = \Theta s + e, \tag{3}$$

where $s = \Psi^{-1}x$ is the sparse coefficient. Here, $\Theta = \Phi\Psi$ can be regarded as a CS measurement matrix to directly observe the sparse coefficient s. More specifically, if the signal is K-sparse, in the circumstances where y is only a linear combination of the K columns of Θ whose corresponding of the sparse coefficients s_i is non-zero. If the priori information that the K entries of the transform coefficient s are non-zero is known, then an $M \times K$ linear system of equations can be obtained to get these non-zero entries. Under this condition, the unknown K equals or less than the number of equations M. Furthermore, the RIP can guarantee that the $M \times K$ system is well-conditioned, which is a necessary and sufficient condition for perfect recovery.

One of the commonly used methods to solve the CS problem (2) or (3) is the l_1-norm minimization with sparsity constraints

$$\min_x \left\{ \frac{1}{2}\|y - \Phi x\|_2^2 + \lambda \|\Psi^{-1}x\|_{l_1} \right\}, \tag{4}$$

or the recovery of the sparse coefficient s

$$\min_s \left\{ \frac{1}{2}\|y - \Phi\Psi s\|_2^2 + \lambda \|s\|_{l_1} \right\}. \tag{5}$$

The first term in the l_1 norm minimization recovery problem (4) or (5) is a penalty term, which is used to calculate the discrepancy between the observation and the solution; the second term is a regularization term, which represents the prior information of the original signal, and λ is an adjustment regularization parameter.

2.2. **The iteration stepsize.** The steepest descent (SD) method [24, 25, 28] is one of the simplest gradient methods for optimization. Its mathematical expression can be given by

$$x_{i+1} = x_i - \beta_i f_i. \tag{6}$$

Here, $f_i = f(x_i)$ represents the gradient vector of arbitrarily object function κ at the current iteration x_i. $\beta_i > 0$ is the iteration stepsize, which should satisfy the following condition

$$\kappa(x_i - \beta_i) = \min_{\beta} \kappa(x_i - \beta f_i). \tag{7}$$

For the function $\kappa = \frac{1}{2}\|\Phi x - y\|_2^2$, it can be obtained that

$$f_i = \Phi^T(\Phi x_i - y), \quad \beta_i = \frac{\|f_i\|_2^2}{(f_i)^T \Phi f_i}. \tag{8}$$

To design a high performance stepsize for superlinear convergence, Barzilai and Borwein [24, 28] use the data in the previous iteration to decide the iteration stepsize in the current iteration. Meanwhile, the iteration (6) can be viewed as

$$x_{i+1} = x_i - D_i f_i. \tag{9}$$

Here, $D_i = \beta_i I$. To guarantee D_i possessing certain quasi-Newton property, it is required to satisfy the following condition

$$\min \left\| s_{i-1} - D_i f'_{i-1} \right\|_2, \tag{10}$$

or

$$\min \left\| D_i^{-1} s_{i-1} - f'_{i-1} \right\|_2. \tag{11}$$

Here, $s_{i-1} = x_i - x_{i-1}$ and $f'_{i-1} = f_i - f_{i-1}$. The following two stepsizes can be obtained from $D_i = \beta_i I$ and the restrictive condition (10) and (11)

$$\beta_i^{BB1} = \frac{s_{i-1}^T f'_{i-1}}{\|f'_{i-1}\|_2^2}, \tag{12}$$

$$\beta_i^{BB2} = \frac{\|s_{i-1}\|_2^2}{s_{i-1}^T f'_{i-1}}. \tag{13}$$

The two stepsizes above are the famous BB stepsizes. Subsequently, to further improve the convergence speed of the SD method, Yuan proposes an improved stepsize β_i^{DY} (Dai-Yuan stepsize) [25] based on the BB stepsizes, so we have

$$\beta_i^{DY} = \begin{cases} \beta_i, & \mathrm{mod}(i,4) = 1 \text{ or } 2 \\ \beta_i^D, & \text{others}, \end{cases} \tag{14}$$

where $\beta_i^D = \frac{2}{\sqrt{(1/\beta_{i-1} - 1/\beta_i)^2 + 4\|f_i\|_2^2/(\beta_{i-1}\|f_{i-1}\|_2)^2} + 1/\beta_{i-1} + 1/\beta_i}$ is a new stepsize. It has been verified that the SD method with Dai-Yuan stepsize converges faster than that with BB stepsizes [25].

3. The Algorithm Research and Design.

3.1. **The classical ICT algorithm.** Curvelet transform [15, 29, 30] is a new geometric multi-scale transform, which has been proved to have better sparse performance than that of wavelet. In addition, the curvelet has excellent identification ability of directions, which make it capable of capturing the image detail features more efficiently. For the image in C^2/C^2 space, it also can provide an efficient, stable and optimized representation [31].

The curvelet transform mainly contains the first generation and the second generation versions. The first generation curvelet is difficult to be implemented due to that its decomposition and synthesis process are more complicated. Subsequently, Candes proposed the second generation discrete curvelt transform [29], which is easier to be used and understood. Unlike the first generation curvelet, the second generation curvelet primarily operates on the frequency domain. What is more, it does not need the ridgelet transform within its achievement process. Additionally, the curvelet coefficients using local Fourier transform can also be directly obtained. In this paper, the second generation curvelt transform is considered as the sparsity transform Ψ.

Different from wavelet which has two parameters, the curvelet contains three parameters. Suppose $x \in R^N$, the curvelet at scale 2^{-j}, orientation θ_l and the position $x_k^{j,l} = R_{\theta_l}^{-1}\left(k_1 \times 2^{-j}, k_2 \times 2^{-j/2}\right)$ can be defined by

$$\varphi_{(j,l,k)}(x) = \varphi_j\left[R_{\theta_l}\left(x - x_k^{(j,l)}\right)\right], \quad l = 0, 1, \ldots \tag{15}$$

where φ is a waveform oscillatory in the horizontal direction and bell-shaped along the vertical direction. R_{θ_l} is a rotation matrix whose rotation angle is $\theta_l = 2\pi \times 2^{-\lceil j/2 \rceil} \times l$ $(0 \le \theta_l \le 2\pi)$ and $R_{\theta_l}^{-1}$ is inverse transform of R_{θ_l}. Since the family of curvelet function builds a tight frame, the following representation can be given for arbitrary function x, i.e.,

$$x = \sum_{(j,l,k)} < x, \varphi_{(j,l,k)} > \varphi_{(j,l,k)}. \tag{16}$$

Here, $< x, \varphi_{(j,lk)} >$ represents the inner product between x and $\varphi_{(j,l,k)}$, which is used to calculate the curvelet coefficients of x.

Let $x_i = x_{i-1} + \mu_i \Phi^T(y - \Phi x_{i-1})$; thus the classical ICT algorithm can be expressed as follows:

$$x_{i+1} = S_{H_W}(x_i) = \sum_{(j,l,k)} H_W\left(< x_i, \varphi_{(j,l,k)} >\right) \varphi_{(j,l,k)}, \tag{17}$$

where μ_i represents the search stepsize, and $H_W(.)$ is the shrinkage threshold operator.

3.2. **The proposed algorithm.** μ_i in the classical ICT algorithm is generally set to 1 for convenience of calculations but affects the convergence speed. Hence, the Dai-Yuan stepsize is applied to the ICT algorithm for accelerating its convergence speed. At the same time, $H_W(.)$ is considered as the curvelet threshold operator [15, 19, 32] is given by

$$H_W(c_\lambda) = \begin{cases} c_\lambda, & |c_\lambda| \ge T \\ 0, & |c_\lambda| < T, \end{cases} \tag{18}$$

where $T = k\sigma_\lambda\sigma$ is the curvelet threshold, and c_λ is the curvelet coefficient. σ represents the standard deviation of noise. σ_λ is the noise standard deviation after curvelet transform, which can be estimated by the Monte-Carlo simulation method [15]. k is a scale-dependent parameter, which is set to 4 for the first scale and 3 for others. It is very simple for setting the value of k. In this paper, a new adjustable parameter $k_1 = \frac{4}{e^{(q-1)/Q}}$ is proposed to adjust the threshold in each iteration. Therefore, a decreasing curvelet threshold can be defined by

$$T = k_1\sigma_\lambda\sigma = \frac{4\sigma_\lambda\sigma}{e^{(q-1)/Q}}, \tag{19}$$

where q is the iteration index and Q is the total number of iterations.

In summary, the proposed algorithm can be summarized as follows.

Step 1: Initialization. Setting the iterative index $q = 1$ and the reconstructed image $x_0 = 0$. After a series of experiments, when the number of iterations is larger than 30, the peak signal to noise ratio (PSNR) and convergence speed of the algorithm proposed

growth are not very obvious. Therefore, to save the reconstruction time, the total number of iterations Q is set to 30.

Step 2: Updating the decreasing curvelet threshold T and the iteration stepsize β_q^{DY}.

Step 3: Calculating the estimation

$$x_q^* = x_{q-1} + \beta_q^{DY}\Phi^T(y - \Phi x_{q-1}). \tag{20}$$

Step 4: Applying the threshold for the estimation

$$x_q = S_{H_S}(x_q^*). \tag{21}$$

Step 5: Adjusting the reconstructed image using the TV method.

$$x_q = x_q - \frac{\partial TV(x_q)}{\partial x_q}.\frac{\mu}{q}, \tag{22}$$

where μ is the TV stepsize. The $TV(x_q)$ can be calculated by

$$TV(x_q) = \sum_{m,n}\sqrt{[x_q(m+1,n) - x_q(m,n)]^2 + [x_q(m,n+1) - x_q(m,n)]^2}.$$

Step 6: If $q \leq Q$, $q = q + 1$ and return to Step 2; else, output the reconstructed image.

4. **The Experiment and Analysis.** In this paper, several simulations are conducted to verify the effectiveness of the algorithm proposed. To assess the performance of the proposed algorithm, it is compared with ICT algorithm, ICT with the decreasing threshold (DICT) [20] and ICT with curvelet hard threshold (CICT). The compression ratio is firstly set to 0.3, and test a 1024×1024 standard Lena image with noise level $\hat{\sigma} = 10$. Figure 1(a) shows the original Lena image. The noisy image is shown in Figure 1(b). Figures 1(c)-1(f) show the recovery image using different algorithms respectively. It can be seen that compared with other three algorithms, the proposed algorithm can effectively suppress the effect of pseudo-gibbs effect and reconstruct a clearer Lena image with relatively higher PSNR. Exclusive inadequacy is the longer reconstruction time (RT).

In terms of astronomical image, compression ratio and the noise level remain unchanged and a 1024×1024 moon image is tested. The reconstructed results from different algorithms are compared in Figure 2. The same conclusion can be obtained that the proposed algorithm is better than other algorithms in terms of PSNR and visual quality since the lunar craters and dark spots in Figure 2(f) are visible clearly while the RT is still longer.

The noise level is kept constant, Figures 3(a) and 3(b) show the PSNR and recovery error from different algorithms when compression ratio changes respectively, which imply that better reconstruction performance with the increase of compression ratio can still be obtained by the proposed algorithm.

The reconstruction time of different algorithms with the increase of compression ratio is compared in Figure 4(a), which implies that as the compression ratio increases, the RT of different algorithms grows longer and longer. However, compared with other algorithms, the proposed algorithm takes longer recovery time. Figure 4(b) shows PSNR of different algorithms as iteration number increases. As comparison, the recovered result of the proposed algorithm with BB stepsize (Proposed+BB) is also presented. It can be seen that the Dai-Yuan stepsize can not only accelerate the convergence speed of the proposed algorithm, but also can improve the algorithm reconstruction performance. Meanwhile, it can be noticed that when iterative number is 30, the PSNR and convergence speed of different algorithms change little.

The Jupiter image is tested, and the compression ratio is considered to be 0.1 and $\hat{\sigma} = 10$. The reconstructed image and evaluation criteria in Figure 5 imply that the proposed algorithm still can obtain high PSNR and better visual effect relatively under

(a) The original image (b) The noisy image (c) ICT, PSNR = 30.18 dB, RT = 9.43 s

(d) CICT, PSNR = 31.87 dB, RT = 11.19 s (e) DICT, PSNR = 32.72 dB, RT = 13.58 s (f) Proposed, PSNR = 35.07 dB, RT = 17.86 s

FIGURE 1. The reconstructed images from different algorithms

(a) The original image (b) The noisy image (c) ICT, PSNR = 29.57 dB, RT = 10.61 s

(d) CICT, PSNR = 31.54 dB, RT = 12.53 s (e) DICT, PSNR = 32.18 dB, RT = 14.17 s (f) Proposed, PSNR = 34.72 dB, RT = 18.34 s

FIGURE 2. The reconstructed images from different algorithms

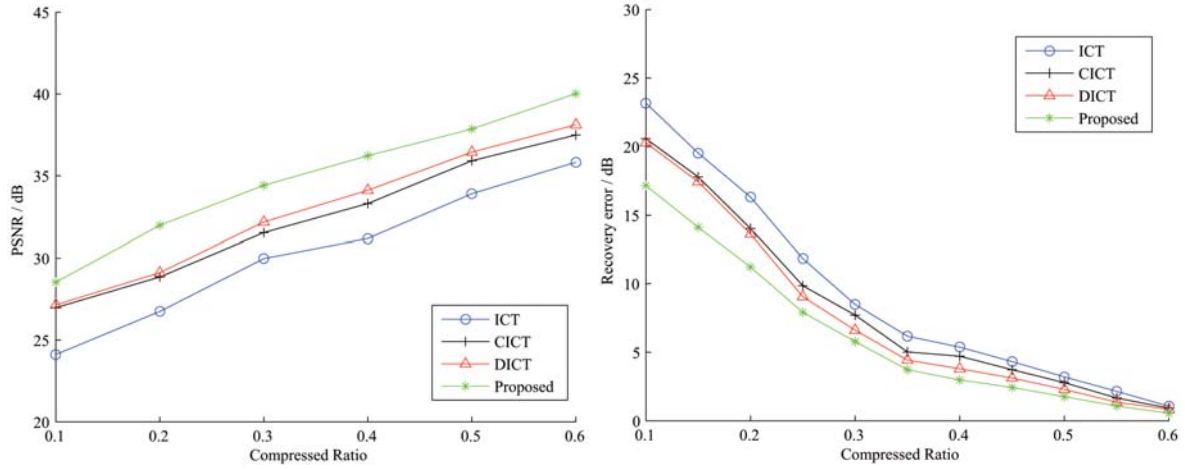

(a) PSNR (b) Recovery error

FIGURE 3. The PSNR (a) and recovery error (b) versus compression ratio

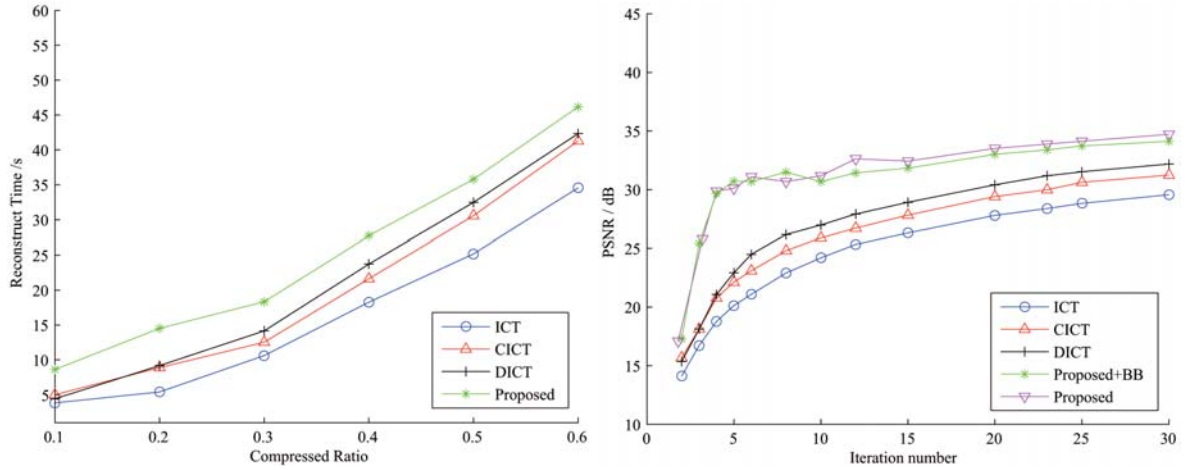

(a) RT (b) PSNR

FIGURE 4. Comparison of the reconstructed results from different algorithms

the circumstances of lower compression ratio. In addition, the gap of reconstruction time between different algorithms is smaller. The same conclusion can also be demonstrated by the objective criteria in Figure 3(a) and Figure 4(a) which imply that the lower compression ratio is, the more obvious the advantage of the algorithm proposed is.

When testing more astronomical images, Tables 1 and 2 show PSNR from different algorithms with the increase of compression ratio and $\hat{\sigma}$ respectively, which demonstrate that the proposed algorithm still can achieve better performance for different astronomical images.

In the research on the reconstruction performance of the proposed algorithm for the detailed feature of astronomical image, a 512×512 local detailed feature image is taken from the original high resolution moon image as the experimental image. Considering that compression ratio is 0.3 and $\hat{\sigma} = 10$, the reconstructed results from DICT and the proposed algorithm are compared in Figure 6.

It can be seen that the proposed algorithm can preserve more astronomical image edge and texture features than DICT.

TABLE 1. PSNR versus compression ratio

Original image	Algorithm	Compression ratio					
		0.1	0.2	0.3	0.4	0.5	0.6
Jupiter	ICT	25.69	27.13	30.15	31.19	33.53	34.62
	CICT	27.07	29.79	32.03	34.28	34.93	36.14
	DICT	27.15	29.43	32.49	34.77	35.82	37.64
	Proposed	30.02	33.21	35.71	36.83	37.94	39.52
Saturn	ICT	24.18	26.64	28.23	30.85	32.13	33.88
	CICT	26.84	29.36	31.52	33.45	34.82	36.29
	DICT	27.01	29.19	32.12	34.37	36.18	37.94
	Proposed	29.63	31.19	33.58	36.41	38.36	40.13
Mars	ICT	25.71	27.94	29.52	30.87	32.02	34.38
	CICT	27.13	28.85	30.34	32.17	35.05	37.63
	DICT	27.86	28.91	31.46	33.82	36.15	38.29
	Proposed	30.12	32.18	34.26	35.92	38.09	40.87

TABLE 2. PSNR versus $\hat{\sigma}$

Original image	Algorithm	$\hat{\sigma}$				
		10	20	30	40	50
Moon	ICT	29.57	29.01	27.82	26.38	24.15
	CICT	31.54	30.93	28.62	27.15	25.84
	DICT	32.18	31.59	30.72	28.94	27.83
	Proposed	34.72	34.15	32.85	31.43	29.67
Jupiter	ICT	30.15	29.67	27.45	25.82	23.83
	CICT	32.03	31.66	29.12	27.13	25.48
	DICT	32.49	31.84	29.69	27.27	25.61
	Proposed	35.71	34.98	32.57	30.16	27.77
Saturn	ICT	28.23	27.74	25.43	24.16	22.08
	CICT	31.52	30.99	28.87	26.19	24.65
	DICT	32.12	31.86	30.62	27.12	25.19
	Proposed	33.58	32.98	30.94	28.96	27.15
Mars	ICT	29.52	29.12	27.19	24.83	22.01
	CICT	30.34	29.83	28.17	26.15	24.16
	DICT	31.46	30.94	29.43	27.28	24.88
	Proposed	34.26	33.53	31.95	29.47	27.76

At the same time, combined with Figure 2 and Figure 6, it can be seen that with the astronomical image resolution reduction, the proposed algorithm can achieve better denoising and reconstruction performance. Meanwhile, it takes relatively less reconstruction time.

5. **Conclusions.** In this paper, the CS theory is applied for solving the problem of high resolution astronomical image denoising. Simultaneously, an iterative curvelet thresholding algorithm with high performance is proposed. The experimental result demonstrates that the proposed algorithm can recover a clear astronomical image with a fast convergence speed. When compression ratio is lower, higher PSNR can still be obtained.

The deep space exploration can benefit from the proposed algorithm. The high resolution astronomical image can be compressed with a lower compression ratio for saving the

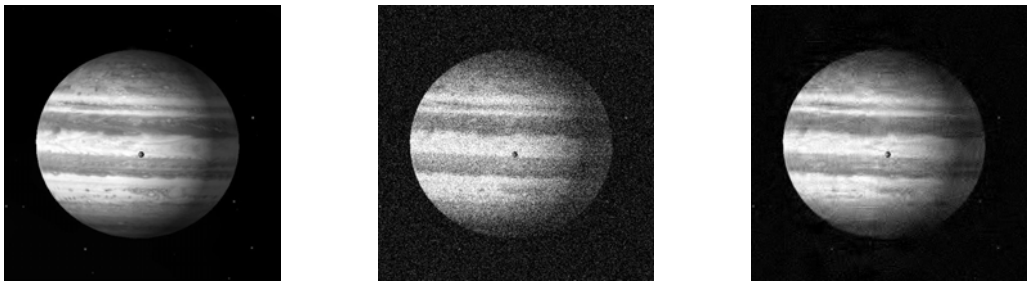

(a) The original image (b) The noisy image (c) ICT, PSNR = 25.69 dB, RT = 5.34 s

(d) CICT, PSNR = 27.07 dB, RT = 7.12 s (e) DICT, PSNR = 27.15 dB, RT = 8.15 s (f) Proposed, PSNR = 30.02 dB, RT = 12.36 s

FIGURE 5. The reconstructed images from different algorithms

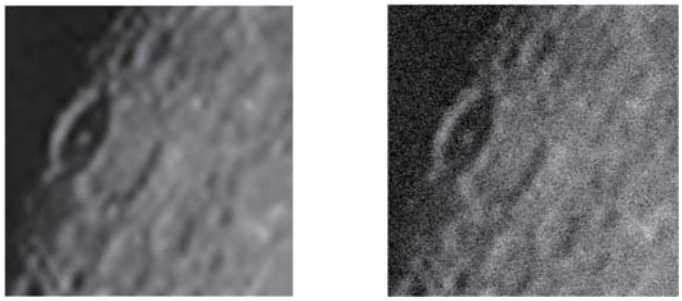

(a) The original image (b) The noisy image

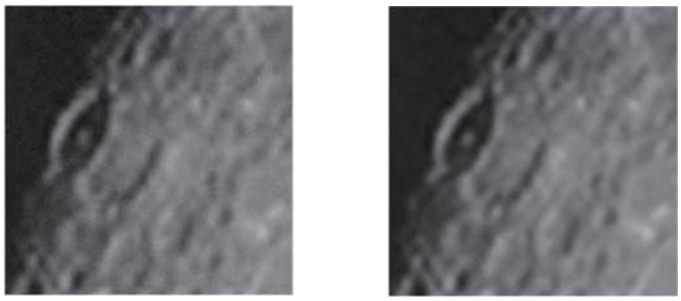

(c) DICT, PSNR = 39.53 dB, RT = 2.48 s (d) Proposed, PSNR = 42.59 dB, RT = 6.78 s

FIGURE 6. The reconstructed images from different algorithms

limited storage space on the satellite or other deep space exploration equipments (such as Mars rover). When the image is transmitted to the ground station, the proposed algorithm can be used to recover a clear high resolution astronomical image. The only drawback to the proposed algorithm is longer reconstruction time. Therefore, how to improve the reconstruction speed is the direction of future efforts.

Acknowledgement. The authors would like to thank Zifa Han and Xiaokun Liu for helping modify the matlab code. The work was supported by the National Natural Science Foundation of China (Grant No. 61427809, 61074127).

REFERENCES

[1] J. J. Benedetto, *Compressed Sensing and Its Applications*, Birkhauser, Switzerland, 2013.
[2] Y. C. Eldar and G. Kutyniok, *Compressed Sensing: Theory and Applications*, Cambridge University Press, New York, 2012.
[3] F. Simon and R. Holger, *A Mathematical Introduction to Compressive Sensing*, Birkhauser, Switzerland, 2013.
[4] X. P. Shi and J. Zhang, Reconstruction and transmission of astronomical image based on compressed sensing, *Journal of System Engineering and Electronics*, vol.27, no.3, pp.680-690, 2016.
[5] D. L. Donoho, Compressed sensing, *IEEE Trans. Information Theory*, vol.52, no.4, pp.1289-1306, 2006.
[6] J. D. Blanchard, J. Tanner and W. Ke, CGIHT: Conjugate gradient iterative hard thresholding for compressed sensing and matrix completion, *Information and Inference*, vol.4, no.4, pp.289-327, 2015.
[7] J. D. Blanchard, J. Tanner and W. Ke, Conjugate gradient iterative hard thresholding: Observed noise stability for compressed sensing, *IEEE Trans. Signal Processing*, vol.63, no.2, pp.528-537, 2015.
[8] Y. D. Zhang, Z. C. Dong, P. Preetha, S. H. Wang, G. L. Ji and J. Q. Yang, Exponential wavelet iterative shrinkage thresholding algorithm for compressed sensing magnetic resonance imaging, *Information Sciences*, vol.322, no.20, pp.115-132, 2015.
[9] Y. D. Zhang, S. H. Wang and G. L. Ji, Exponential wavelet iterative shrinkage thresholding algorithm with random shift for compressed sensing magnetic resonance imaging, *IEEE Trans. Electrical and Electronic Engineering*, vol.10, no.1, pp.116-117, 2015.
[10] E. Candes and T. Tao, Decoding by linear programming, *IEEE Trans. Information Theory*, vol.51, no.12, pp.4203-4215, 2005.
[11] Y. Plan and V. Roman, One-bit compressed sensing by linear programming, *Communications on Pure and Applied Mathematics*, vol.66, no.8, pp.1275-1297, 2013.
[12] F. Jun, J. Li and Y. N. Shen, Super-resolution compressed sensing: An iterative reweighted algorithm for joint parameter learning and sparse signal recovery, *IEEE Signal Processing Letters*, vol.21, no.6, pp.761-765, 2014.
[13] F. Liu, L. P. Li and L. C. Jiao, Nonconvex compressed sensing by nature-inspired optimization algorithms, *IEEE Trans. Cybernetics*, vol.45, no.5, pp.1028-1039, 2015.
[14] J. D. Blanchard, C. Michael and H. David, Greedy algorithms for joint sparse recovery, *IEEE Trans. Signal Processing*, vol.62, no.7, pp.1694-1704, 2014.
[15] J. L. Starck, E. J. Candes and D. L. Donoho, The curvelet transform for image denoising, *IEEE Trans. Image Processing*, vol.11, no.6, pp.670-683, 2002.
[16] S. Elaiwat, M. Bennamoun and F. Boussaid, 3-D face recognition using curvelet local features, *IEEE Signal Processing Letters*, vol.21, no.2, pp.172-175, 2014.
[17] H. Cui and G. B. Yan, Improved curvelet thresholding denoising method by the chi-squared cumulation distribution distribution function and PDE, *Journal of Xidian University*, vol.41, no.4, pp.108-110, 2014.
[18] Y. Zhang, W. J. Ren and G. W. Tang, Algorithm of image compressed sensing reconstruction based on curvelet sparese representation, *Control and Instruments in Chemical Industry*, vol.42, no.11, pp.1206-1210, 2015.
[19] J. W. Ma, A single-pixel imaging system for remote sensing by two-step iterative curvelet thresholding, *IEEE Geoscience and Remote Sensing Letters*, vol.6, no.4, pp.676-680, 2009.
[20] J. W. Ma and F. X. Dimet, Deblurring from highly incomplete measurements for remote sensing, *IEEE Trans. Geoscience and Remote Sensing*, vol.47, no.3, pp.792-802, 2009.

[21] Y. Zhang, J. W. Ren and G. W. Tang, Algorithm of compressed sensing reconstruction of seismic data based on curvelet transform, *Journal of Jilin University (Information Science Edition)*, vol.33, no.5, pp.570-577, 2015.

[22] W. Liu, S. Y. Cao and Z. Cui, Random noise attenuation based on compressive sensing and TV rule, *Geophysical Prospecting for Petroleum*, vol.54, no.2, pp.181-187, 2015.

[23] J. J. Cao, J. T. Zhao and Z. Y. Hu, 3D seismic denoising based on a low-redundancy curvelet transform, *Journal of Geophysics and Engineering*, vol.12, no.4, pp.566-576, 2015.

[24] J. Barzilai and J. M. Borwein, Two point step size gradient methods, *IMA Journal of Number Analysis*, vol.8, no.1, pp.141-148, 1988.

[25] Y. Yuan, A new stepsize for the steepest descent method, *Journal of Computational Mathematics*, vol.24, no.2, pp.149-156, 2006.

[26] L. Lin, L. F. Kong and Q. S. Lian, Image compressed sensing reconstruction based on contourlet Wiener filtering, *Chinese Journal of Scientific Instrument*, vol.30, no.10, pp.2052-2056, 2009.

[27] V. Voroniski and Z. Q. Xu, A strong restricted isometry property, with an application to phaseless compressed sensing, *Applied and Computational Harmonic Analysis*, vol.40, no.2, pp.386-395, 2016.

[28] Y. Dai and Y. Yuan, Analysis of monotone gradient method, *Journal of Industrial and Management Optimization*, vol.1, no.2, pp.181-192, 2005.

[29] H. Z. Yang and L. X. Ying, Synchrosqueezed curvelet transform for two-dimensional mode decomposition, *SIAM Journal on Mathematical Analysis*, vol.16, no.3, pp.2052-2083, 2014.

[30] G. Q. Gu, K. F. Wang and X. Xu, Denoising in digital speckle pattern interferometry using fast discrete curvelet transform, *The Imaging Science Journal*, vol.62, no.2, pp.106-110, 2013.

[31] W. Li and H. Yang, Curvelet domain empirical Wiener filter, *Journal of Jilin University (Science Edition)*, vol.51, no.2, pp.313-316, 2013.

[32] R. A. Ansari and B. K. Mohan, Noise filtering of remotely sensed images using iterative thresholding of wavelet and curvelet transforms, *The International Archives of Photogrammetry, Remote Sensing and Spatial Information Sciences*, vol.XL-1, no.17, pp.57-64, 2014.